Automated microaneurysm detection method based on double-ring filter and feature analysis in retinal fundus images

Yuji Hatanaka, Tsuyoshi Inoue, Susumu Okumura, Chisako Muramatsu* and Hiroshi Fujita*
School of Engineering, The University of Shiga Prefecture, Japan
**Graduate School of Medicine, Gifu University, Japan*
hatanaka.y@usp.ac.jp

Abstract

Microaneurysm in the retina is one of the signs of simple diabetic retinopathy. We have been investigating a computerized method for the detection of microaneurysms on retinal fundus images. In this study, the computerized scheme was developed by using twenty five cases. After image preprocessing, candidate regions for microaneurysms were detected using a double-ring filter. Any potential false positives located in the regions corresponding to blood vessels were removed by automatic extraction of blood vessels from the images. One hundred twenty six image features were determined, and 28 components were selected by using principal component analysis, and the candidate lesions were classified into microaneurysms or false positives using the rule-based method and an artificial neural network. The true positive rate of the proposed method was 68% at 15 false positives per image.

1. Introduction

In Japan, there are approximately 8.9 million patients with confirmed diabetes and approximately 22.1 million patients with suspected diabetes. Approximately 3 million are thought to suffer from diabetic retinopathy (DR). This disease can be prevented from causing blindness if it is treated at an early stage. However, approximately 3,000 people have lost their vision following the onset of DR. The ophthalmologists diagnose DR by finding hemorrhages, microaneurysms, and exudates in retinal fundus images. The contrast of hemorrhages and microaneurysms are increased by using fluorescein angiograms. However, using fluorescein for diagnosing DR is not feasible in the case of mass screening. Thus it is desirable to detect hemorrhages and microaneurysms on retinal fundus images without using the contrast medium; however, detection of hemorrhages and microaneurysms is difficult because of their low contrast in noncontrast images. Therefore, a computer-aided diagnosis (CAD) system for the detection of these lesions can help physicians who review the mass screening exams in diagnosing DR.

Usher et al. reported a method for detecting hemorrhages, microaneurysms, and exudates by using adaptive intensity thresholding combined with an edge enhancement operation [1]. Niemeijer et al. proposed a method for the detection of red regions by pixel classification and feature analysis [2]. Grisan et al. proposed a method for detecting the dark lesions on the basis of local thresholding and pixel density [3]. Niemeijer et al. held the first international microaneurysm detection competition, organized in the context of the Retinopathy Online Challenge (ROC), a multiyear online competition for various aspects of DR detection [4]. Thus, several studies using ROC database were reported. Xu et al. reported a method for detecting microaneurysms based on mathematical morphological black top hat and their feature [5]. Their features extracted were classified by support vector machine. Zhang et al. proposed a microaneurysms detection method using multi-scale Gaussian correlation filtering and sparse representation classifier [6]. Antal et al. proposed a microaneurysms detection method based on ensemble using features [7]. We also proposed a method based on double ring filter in noncontrast images of the retinal fundus [8]. But, the previous method caused many false positives, thus the aim of the present study is to improve the previous method.

2. Method

ROC database were used in this study. For ROC competition, they compared the results of five different methods, produced by five different teams of researchers on the same set of data. The database includes 50 retinal fundus images with "gold standard" locations of microaneurysms identified by a consensus of four ophthalmologists; these cases were intended to be used as a training set for the development of CAD systems. The ROC also includes 50 testing cases in which "gold standard" locations are not provided to the

978-1-4673-2051-1/12/$31.00 ©2012 IEEE

participants. For this reason, even though the results for the test cases are also included, training cases are mainly discussed in this paper. The 50 training cases include RGB color images in three different image sizes. In this study, we selected 25 images with the highest resolution; 1389 × 1388 pixels. Nineteen images include a total of 156 microaneurysms, whereas no microaneurysms were identified in the remaining 6 images. The number of microaneurysms identified in each of the 19 images ranges from 1 to 41. Twenty-three images also include a total of 136 hemorrhages of untargets in this study, whereas no hemorrhages were identified in the remaining 2 images.

2.1. Overall scheme for detection of microaneurysms

A lesion appears darker than the surrounding regions in retinal fundus images as shown in Figure 1. Thus, our previous method [8] focused on a contrast between both regions. First, images were preprocessed to reduce noise and variation in the brightness of the images. The initial detection of the microaneurysms was attempted by applying the double-ring filter on the green channel of the color images. The blood vessels were then removed. However, our previous method could not remove any blood vessels, thus this step was improved in this study. Next, the shapes of the candidate lesions for an accurate determination of their image features were examined. Finally, the candidate lesions were classified as microaneurysms or false positives by the rule-based method and by using an artificial neural network (ANN). In final step, our previous method misclassified many false positives as the microaneurysms. Therefore, the features based on texture analysis were added in this study.

2.2. Initial detection of microaneurysms

The differences in brightness and colors of the retinal fundus images were due to the photographic conditions. In order to reduce these differences, brightness correction [9], gamma correction, and histogram expansion were applied to each image. The contrast of microaneurysms tends to be high in green color; therefore, RGB color images were converted to green-channeled images. Because the image noise may also be amplified, a low-pass filter based on FFT (Fast Fourier Transform) was applied for reducing the image noise.

Microaneurysms appear as lesions darker than the surrounding retinal regions. Therefore, it was expected that microaneurysms could be detected by using a double-ring filter A [10], which compares the target

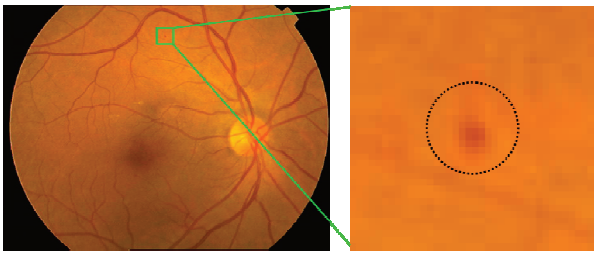

(a) (b)

Figure 1. Example of a retinal fundus image with a microaneurysm. (a) Original retinal fundus image, and (b) enlarged image of the microaneurysm marked by a rectangle in (a).

pixel values with the neighboring pixel values. The filter consists of an inner circle and an outer ring with diameters of 5 and 13 pixels, respectively. An inner circle is defines as a region A. A rim width of outer ring is 2 pixels, and it is defined as a region C. A region B is a gap with 2 pixels widths, which is not used for filtering because this region is affected by a microaneurysm edges. The output value of this filter is follow as

$$F_A(x, y) = 128 - (k(x, y) - m_A(x, y)) \quad (1)$$

where m_A is mean in a region A and $k(x, y)$ is a pixel value of p% of a histogram in a region C. If the F_A was high, the pixel in question became a candidate pixel for microaneurysms. In this study, the maximum number of candidate lesions for microaneurysms in each image was limited to 275.

2.3. Removal of blood vessels appearing as false positives

After the initial detection of microaneurysms, many blood vessels appeared as false positives in the preprocessed green-channeled images. In order to eliminate these false positives, the pixels corresponding to the part of the blood vessels (BVs) were extracted by using the method combined with double-ring filter B and black-top-hat-transform because Muramatsu et al. reported that the BVs were extracted effectively by combining with two methods [11]. A structure of double ring filter B was different than filter A. The output value of this filter is follow as

$$F_B(x, y) = 128 - (m_{BB}(x, y) - m_{AB}(x, y)) \quad (2)$$

where m_{AB} and m_{BB} are means in region A and region B, respectively. The initially detected candidates were superimposed onto the images of the extracted blood

vessels. Lesions that were detected in the blood vessel regions were considered as false positives and removed from the candidates.

2.4. Re-examination of candidate lesions

The shapes of candidate lesions after the initial detection are affected by the structure of the double-ring filter. Therefore, the shapes of candidate lesions were not determined accurately, which could influence the accuracy of image feature analysis. In order to determine the shapes of candidate lesions correctly, their shapes were re-examined. On the basis of the remaining candidate pixels after the removal of false positives, neighboring pixels with comparable pixel values were included in the candidate lesions.

2.5. Feature determination and reduction of false positives

The candidate lesions in the initial detection process included numerous false positives. Therefore, in order to remove the false positives, 126 image features were calculated. These features included (1) area, (2) degree of circularity, (3) length-to-width ratio [16], (4-6) mean value of the candidate lesion in each of the red, green, and blue bits, (7-9) difference between the maximum and minimum pixel values of the candidate lesion in each of the red, green, and blue bits, and (10-12) contrast, (13) similarity of BV, (14) number of labels in binarized image, (15) variance in pixel values, (16) nearest distance from BVs, (17) RMS(Root Mean Square), (18) 1st moment, (19, 20) ordinate and abscissa from optic disc, (21-23) values of double ring filter [10] in R, G, B values, (24-26) values of double ring filter A in R, G, B values, (27- 126) features based on texture analysis added in this study.

In features (27-78), angular second moment, contrast, correlation, variance, inverse difference moment, sum average, sum variance, sum entropy, entropy, difference variance, difference entropy, and s kinds of information measure of correlation were calculated from co-occurrence matrix. In features (79-86), angular second moment and mean were calculated from gray level difference statistics. In features (87-126), short runs emphasis, long runs emphasis, gray level nonuniformity, run length nonuniformity, and run percentage were calculated from 0 and 90 degrees of run length matrixes.

On the basis of these features, candidate lesions were classified as microaneurysms or false positives using the rule-based method and an ANN. For the ANN, 126 features were transformed to 28 components by principal component analysis (PCA). The ANN with a three-layered feed-forward network was learned by using a back-propagation algorithm. The number of hidden units was varied experimentally. For avoiding over-training of the ANN, the training was stopped at a certain iteration number.

3. Results and discussion

The proposed method was evaluated by use of the free-response receiver operating characteristic (FROC) analysis. The ROC database includes many microaneurysms that are very difficult to detect. Therefore, the visibilities of the microaneurysms used in this study were evaluated individually by the two researchers in this study. As a result, 84 out of 156 microaneurysms, 54 percent of all, were determined invisible by both researchers. Therefore, for the training cases, the results of the poposed method were evaluated in two ways: the sensitivities were determined for all microaneurysms and for visible microaneurysms only.

For evaluation of trained ANN, ANN was evaluated by using leaven one out cross validation in seventy six microaneurysms detected and 4315 false positives. The ANN's parameters were set when area under the curve (AUC) in receiver of characteristic (ROC) analysis was max. The true positive fractions (TPFs) and the number of false positives per image (FPI) by the initial detection, the classification by the ANN using 126 features, and the previous method are summarized in Table 1. The TPFs for the 84 visible microaneurysms are also shown in Table 1. The results indicate that detection of microaneurysms in the images of the ROC database is very difficult. But, the proposed method

Table 1. True positive fractions (TPFs) and the numbers of false positives per image (FPI) after the initial detection process, false positive reduction using the rule-based method and ANN.

	TPF of all microaneurysms	TPF of visible microaneurysms	FPI
Initial detection	0.487 (76 / 156)	0.699 (59 / 84)	173 (4315 / 25)
Reduction of false positives	0.397 (62 / 156)	0.682 (58 / 84)	15 (385 / 25)
Previous method [8]	0.417 (65 / 156)	0.682 (58 / 84)	26 (641 / 25)

was improved by reduction of false positives based on texture analysis.

Figure 2 shows FROC curves obtained for all microaneurysms and only visible ones. It is apparent in Figure 2 that the sensitivity for detecting visible microaneurysms was considerably higher than that for "invisible" microaneurysms. Moreover, the proposed method was higher than the previous one slightly.

False positives detected can be grouped into two major categories: (1) capillary blood vessels not to be identified as the blood vessels, and (2) noise regions. Because the accuracy of the extraction of blood vessels was insufficient, reduction of some false positives in the blood vessel regions failed. The accuracy of extraction of large blood vessels was relatively high, whereas it was low for the capillary blood vessels. In order to remove the false positives in the blood vessels, it is important to improve the accuracy of extraction of blood vessels.

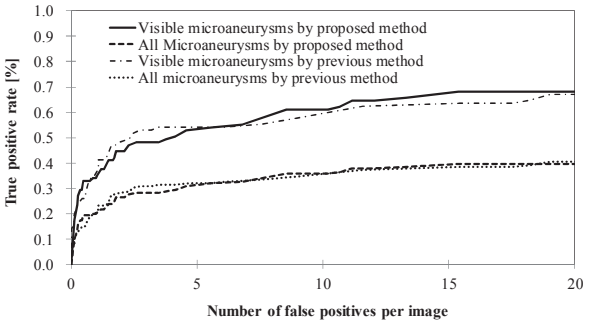

Figure 2. FROC curves for all microaneurysms and only visible microaneurysms.

4. Conclusion

We investigated a method for the automated detection of microaneurysms on retinal fundus images. We applied our method on the 25 cases obtained from the ROC database; the sensitivity of our method was 68% with the 15 false positives per image. Although proposed method has several problems, our method could be improved further for the detection of visible microaneurysms in order to facilitate the early diagnosis of DR.

Acknowledgements

This study was supported in part by a grant for the Grant-in-Aid for Young Scientists (B) from the Ministry of Education, Culture, Sports, Science and Technology, Japan. The authors thank A. Mizutani for their significant contributions to this study.

References

[1] D. Usher, M. Dumskyj, M. Himaga, T. H. Williamson, S. Nussey and J.F. Boyce, "Automated detection of diabetic retinopathy in digital retinal images: a tool for diabetic retinopathy screening", *Diabetic UK Diabetic Medicine*, vol. 21, no. 1, pp. 84–90, Jan. 2004.

[2] M. Niemeijer, B. van Ginneken, L. Staal, M. S. Suttorp-Schulten and A. D. Abramoff, "Automatic detection of red lesions in digital color fundus photographs", *IEEE Trans. Med. Imag.*, Vol. 24, no. 5, pp. 584–592, May 2005.

[3] E. Grisan and A. Ruggeri, "Segmentation of candidate dark lesions in fundus images," *Proc. 29th IEEE EMBS*, pp. 6735-6738, Aug. 2007.

[4] M. Niemeijer, B. van Ginneken, M. J. Cree, A. Mizutani, G. Quellec, C. I. Sanchez, B. Zhang, R. Hornero, M. Lamard, C. Muramatsu, X. Wu, G. Cazuguel, J. You, A. Mayo, Q. Li, Y. Hatanaka, B. Cochener, C. Roux, F. Karray, M. Garcia, H. Fujita and M. D. Abramoff, "Retinopathy online challenge: Automatic detection of microaneurysms in digital color fundus photographs", *IEEE Trans. Med. Imag.*, vol. 29, no. 1, pp. 185-195, Jan. 2010.

[5] L. Xu, S. Luo, "Optimal algorithm for automatic detection of microaneurysms based on receiver operating characteristic curve," *J. Biomedical Optics,* vol. 15, no. 6, pp. 065004-1-6, Dec. 2010.

[6] B. Zhang, K. Karray, L. Zhang, J. You, "Microaneurysm (MA) Detection via Sparse Representation Classifier with MA and Non-MA Dictionary Learning, "*2010 International Conference on Pattern Recognition*, pp. 277-280, Aug. 2010.

[7] B. Antal, and A. Hadju, "An ensemble-based microaneurysm detector for retinal images," *Proc. 18th IEEE ICIP*, pp. 1621-1624, Sept. 2011.

[8] A. Mizutani, C. Muramatsu, Y. Hatanaka, S. Suemori, T. Hara and H. Fujita, "Automated microaneurysm detection method based on double-ring filter in retinal fundus images," *Proc. SPIE*, vol. 7260, pp. 72601N-1-8, Feb. 2009.

[9] Y. Hatanaka, T. Nakagawa, Y. Hayashi, M. Kakogawa, A. Sawada, K. Kawase, T. Hara and H. Fujita, "Improvement of Automatic Hemorrhages Detection Methods using Brightness Correction on Fundus Images", *Proc. SPIE*, vol. 6915, pp. 69153E-1-10, Feb. 2008.

[10] Y. Hatanaka, T. Nakagawa, Y. Hayashi, A. Aoyama, X. Zhou, T. Hara, H. Fujita, Y. Mizukusa, A. Fujita and M. Kakogawa, "Automated detection algorithm for arteriolar narrowing on fundus images", *Proc. 27th IEEE EMBS*, pp. 286-290, Aug. 2005.

[11] C. Muramatsu, Y. Hatanaka, T. Iwase, T. Hara and H. Fujita, "Automated selection of major arteries and veins for measurement of arteriolar-to-venular diameter ratio on retinal fundus images", *Computerized Medical Imaging and Graphics*, vol. 35, no. 6, pp. 472-480, Sept. 2011.